An efficient transition path sampling algorithm for nanoparticles under pressure

Cite as: J. Chem. Phys. **127**, 154718 (2007); https://doi.org/10.1063/1.2790431
Submitted: 12 June 2007 . Accepted: 04 September 2007 . Published Online: 18 October 2007

Michael Grünwald, Christoph Dellago, and Phillip L. Geissler

An efficient transition path sampling algorithm for nanoparticles under pressure

Michael Grünwald and Christoph Dellago[a)]
Faculty of Physics, University of Vienna, Boltzmanngasse 5, 1090 Vienna, Austria and Center for Computational Materials Science, University of Vienna, Boltzmanngasse 5, 1090 Vienna, Austria

Phillip L. Geissler
Department of Chemistry, University of California at Berkeley, Berkeley, California 94720, USA

(Received 12 June 2007; accepted 4 September 2007; published online 18 October 2007)

We apply transition path sampling to the simulation of nanoparticles under pressure. As a barostat we use a bath of ideal gas particles that form a stochastically updated atmosphere around the nanoparticle. We justify this algorithm by showing that it preserves the distribution of an ideal gas at constant temperature and pressure by satisfying detailed balance. Based on this result, we present a simple and efficient transition path sampling scheme for the study of activated processes in nanoparticles under pressure. As a first application, we investigate the *h*-MgO to rocksalt transformation in faceted CdSe nanocrystals. Starting from an artificial mechanism involving a uniform motion of all atoms, trajectories quickly converge towards the dominant mechanism of nucleation and growth along parallel (100) planes. © *2007 American Institute of Physics*.
[DOI: 10.1063/1.2790431]

I. INTRODUCTION

The physical and chemical properties of nanoscale matter are dominated by surface effects and can deviate from the properties of the bulk material in both quantitative and qualitative ways. For instance, pressure-induced structural phase transformations show strong dependence on particle size: nanocrystals transform at higher pressures and show much stronger hysteresis than the corresponding bulk materials.[1–6] Furthermore, the enhanced role of surface free energy can generate unique structural transformation mechanisms and stabilize crystal structures that are unstable in the bulk.[7]

Molecular dynamics computer simulations can play a key role in identifying the atomistic details of pressure-induced structural transformations in nanocrystals[7–14] as well as in the bulk.[15–17] An important issue in the simulation of nanoparticles under pressure is the method through which hydrostatic pressure is applied. While methods exist that allow pressurization of a nanoparticle in vacuum,[18] an explicit pressure medium must be included to model the experimental situation more closely. Two main methods have been proposed so far: In the first, the medium consists of Lennard-Jones particles and the pressure is controlled by a variant of the extended Lagrangian approach,[9–12,14,18] changing the dynamics of the particles. In the second method, the pressure medium is made up of soft sphere particles, for which the equation of state is known.[8,18] Here, the pressure is controlled by a single parameter of the interaction potential, although the volume accessible to the pressure medium, a necessary parameter for exactly tuning the pressure, can only be estimated. In both methods, special care must be taken in choosing the parameters of the pressure medium: for the exerted pressure to be hydrostatic, the dynamics of the pressure medium must not slow down significantly even at pressures of tens of gigapascal.

In our simulations we use a recently developed ideal gas barostat,[7,19] where the nanoparticle is surrounded by a thin atmosphere of noninteracting particles that are stochastically introduced on the surface of the atmosphere, with appropriate statistics for an ideal gas at the desired temperature and pressure. In this approach, the pressure is easily controlled by adjusting the number of gas particles in the simulation. Furthermore, there is no need for an additional thermostat because the temperature of the system is set by the gas particles' velocity distribution. As there are no interactions in the gas, the exerted pressure is ideally hydrostatic at all times.

The ideal gas barostat seems intuitively correct and can be implemented efficiently in a simulation. Yet, its usefulness can only be established by showing that it indeed preserves the distribution of a system at constant pressure and temperature. While such a demonstration is straightforward for simple algorithms, complications arise in our case due to the stochastic nature of the pressure bath. As the number of gas particles in the simulation is not constant and particles may be added or removed from the simulation in different ways, a careful analysis of the different steps of the algorithm is necessary.

In this paper, we show that the ideal gas barostat, appropriately implemented, satisfies detailed balance and therefore preserves the correct equilibrium distribution of a nanocrystal immersed in an ideal gas at constant temperature and pressure. This result allows us to implement a simple transition path sampling scheme[20,21] for the simulation of activated processes in nanoparticles under pressure. We apply the algorithm to study the recently observed mechanism of the

[a)]Electronic mail: christoph.dellago@univie.ac.at

h-MgO to rocksalt transformation[7] in a model of faceted CdSe nanocrystals at the bulk transition pressure of 2.5 GPa. Starting from a trajectory displaying a transformation mechanism previously suggested by Tolbert and Alivisatos,[1] the simulation quickly finds its way to the primary mechanism, which involves the sliding of parallel (100) planes.

The paper is organized in the following way. In Sec. II we review the details of the ideal gas pressure bath and rewrite the algorithm in a way suitable for further analytical treatment. Section III contains the proof of detailed balance for this algorithm. Based on this result, we present an efficient transition path sampling algorithm for nanoparticle and pressure bath in Sec. IV. A discussion of our simulation results on CdSe nanocrystals is given in Sec. V.

II. IDEAL GAS PRESSURE BATH

Our pressure bath consists of particles that do not interact with each other, but interact with atoms in the nanoparticle by a repulsive soft sphere potential of the form

$$u(r) = \begin{cases} \epsilon[(r/\sigma)^{-12} - (r_{\text{cut}}/\sigma)^{-12}] & \text{if } r < r_{\text{cut}} \\ 0 & \text{if } r \geqslant r_{\text{cut}}. \end{cases} \quad (1)$$

We set $\epsilon = 1$ kJ/mol and choose σ large enough to prevent gas particles from penetrating the nanoparticle (for CdSe nanocrystals a value of 3 Å is sufficient); we cut the potential at a value of $r_{\text{cut}} = 2\sigma$. To compute the forces between gas and crystal, we use the cell list method[22] with cells of side-length $l_{\text{cell}} = r_{\text{cut}} + 0.1$ Å.

The gas particles fill a thin atmosphere around the nanocrystal. Using the cell list method, it is convenient to define this atmosphere as consisting of all cells that can hold possible interaction partners of crystal atoms. Thus, the outer boundary of the ideal gas atmosphere consists of flat rectangular parts. Gas particles that leave this atmosphere are no longer considered while new particles are introduced on the surface of the atmosphere with the correct statistics for an ideal gas at pressure P and temperature T. The equations of motion of all particles are integrated using the velocity Verlet algorithm.[22] Note that the stochastic treatment of the pressure bath bears some resemblance to an existing method for modeling solvent dynamics.[23]

The following algorithm differs in some details from the one presented in an earlier paper,[19] which for subtle reasons does not precisely satisfy detailed balance (for a discussion of this issue, see Sec. III D). However, we have verified that results obtained using the old version[7,19] remain unchanged when using the correctly balanced algorithm enumerated below and depicted in Fig. 1.

(1) Propagate the positions of the crystal atoms for one time step (first step of the velocity Verlet algorithm).
(2) Check if the boundaries of the atmosphere must change due to movement of crystal atoms. Remove cells and gas particles therein that are no longer needed.
(3) Propagate the positions of the gas atoms for one time step (first step of the velocity Verlet algorithm). Note that for this step forces obtained with the crystal atoms in their original position, i.e., before step 1, are used. Remove all gas particles that have left the atmosphere. Place n_{in} gas particles on the surface of the atmosphere, with positions drawn from a uniform distribution. n_{in} ("in" for "inject") is a number drawn from a Poisson distribution with an average of

$$\bar{n}_{\text{in}} = (2\pi m k_{\text{B}} T)^{-1/2} A P \Delta t, \quad (2)$$

where m is the mass of the gas particles, k_B is the Boltzmann constant, T and P are the desired temperature and pressure, A is the total surface area of the atmosphere, and Δt is the time step. Let $\mathbf{n}_x$ denote the local unit normal to the surface pointing into the system. The

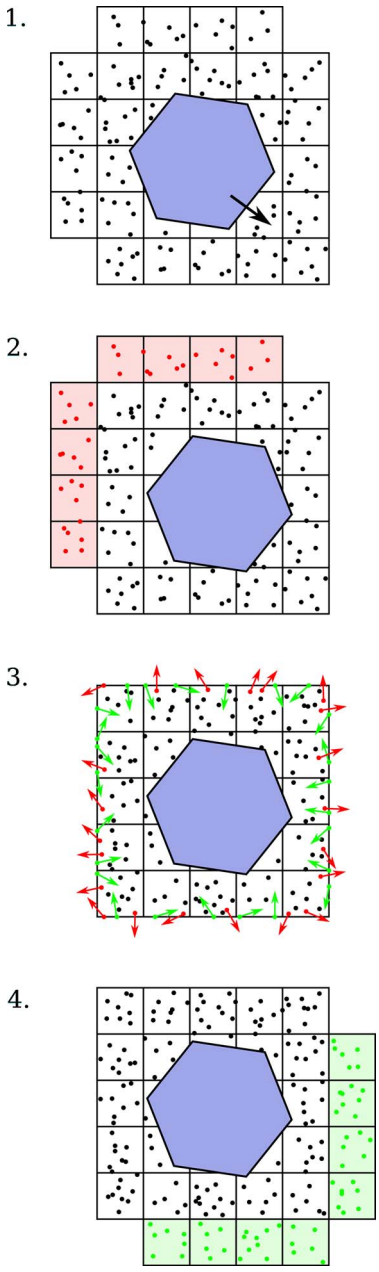

FIG. 1. Illustration of the ideal gas algorithm. (1) Propagate crystal atoms (blue). (2) If necessary, remove cells and gas particles therein that are no longer needed (red). (3) Propagate gas atoms and remove those (red) that leave the atmosphere. Put new gas particles (green) on the surface and propagate them into the atmosphere; remove those (red) that end up outside. (4) If necessary, add new cells and fill them with gas particles (green).

velocity distribution in that direction is given by

$$p(v_x) = \frac{m}{k_B T} v_x \exp\left(-\frac{m v_x^2}{2 k_B T}\right). \tag{3}$$

The velocity distribution in directions perpendicular to $\mathbf{n}_x$ is Maxwell-Boltzmann. To take into account that the gas particles will not enter the atmosphere all at the same time but instead at a variety of times equally distributed over the period of one time step, propagate them for a random time step between zero and Δt, drawn from a uniform distribution. Keep only those particles that stay within the boundary of the atmosphere.

(4) If necessary, add new cells and fill them with N_{app} gas particles. N_{app} ("app" for "appear") is a number drawn from a Poisson distribution with an average of

$$\bar{N}_{\mathrm{app}} = \frac{P V_{\mathrm{app}}}{k_B T}, \tag{4}$$

where V_{app} is the total volume of all added cells. The positions of the particles are uniformly distributed over the cell volume and their velocity distribution is Maxwell-Boltzmann.

(5) Compute forces and propagate all velocities of crystal and gas atoms (second step of the velocity Verlet algorithm).

The algorithm propagates the system, nanocrystal, and pressure bath, for one time step.

III. DETAILED BALANCE FOR THE IDEAL GAS BAROSTAT

In the following we show that the algorithm presented in Sec. II conserves the correct equilibrium distribution of a nanocrystal immersed in an ideal gas at constant pressure and temperature by satisfying a detailed balance condition.

The stationary distribution that the algorithm should conserve is that of a system at constant chemical potential μ, pressure P, and temperature T, where μ is given by an equation of state $\mu(P,T)$. Fixing only these intensive parameters, no constraint is put on extensive parameters such as the number of particles N, the volume V, and the energy U. However, the volume of the system is determined by the external condition that the atmosphere of ideal gas particles around the nanoparticle be as small as possible. Thus, a constant μPT ensemble is realized, and the desired stationary distribution is given by

$$\rho(x) \propto \frac{1}{h^{3N}} e^{-\beta(U+PV-\mu N)}, \tag{5}$$

where x denotes the microscopic physical state of the system consisting of the positions and momenta of all particles, h is Planck's constant, and $\beta = 1/k_B T$.

A sufficient condition for the conservation of $\rho(x)$ is the detailed balance condition[24]

$$\frac{p(x-x')}{p(\bar{x}'-\bar{x})} = \frac{\rho(x')}{\rho(x)}, \tag{6}$$

where $p(x-x')$ is the probability to go from physical state x to state x' by the rules of the underlying dynamics and states $\bar{x}$ and $\bar{x}'$ are obtained by inverting the momenta in states x and x', respectively. In the following we explicitly calculate $p(x-x')$ for the ideal gas barostat and show that Eq. (6) holds.

A. Combinatorics

As a first step, we cast Eq. (6) into a form that takes into account the fact that a single physical state x can have different representations in a computer simulation.

Let x denote the physical state of a classical system of N indistinguishable particles, which of course makes no reference to which particle is which. In a computer simulation we cannot avoid keeping a list of particle positions in some order. As a result, one physical state is represented by $N!$ "computer" states x_P, each corresponding to a distinct permutation of the stored list of positions, i.e.,

$$x \equiv \{x_1, x_2, \ldots, x_{N!}\}. \tag{7}$$

Taking this degeneracy of the physical state x into account, the stationary distribution of computer states is given by

$$\rho(x_P) = \frac{\rho(x)}{N!}. \tag{8}$$

To determine the total rate of transitions $W(x-x')$ from one physical state x to another x', we must consider all moves $x_P - x'_{P'}$ that are allowed by a given sampling algorithm as follows:

$$W(x-x') = \sum_P \sum_{P'} w(x_P - x'_{P'}). \tag{9}$$

Here $w(x_P - x'_{P'})$ is the transition rate for a specific pair of computer states, depending on the time step Δt, the distribution of computer states $\rho(x_P)$, and the conditional probability $p(x_P - x'_{P'})$ that a simulation at x_P will move to $x'_{P'}$ in a single step,

$$w(x_P - x'_{P'}) = \frac{1}{\Delta t} \rho(x_P) p(x_P - x'_{P'}). \tag{10}$$

It seems that in any reasonable algorithm the way a physical state x is treated should not depend on the order in which particle positions are stored, so $\rho(x_P)$ and $\Sigma_{P'} w(x_P - x'_{P'})$ do not depend on P. We can therefore write

$$\begin{aligned} W(x-x') &= \frac{1}{\Delta t} N! \rho(x_1) \sum_{P'} p(x_1 - x'_{P'}) \\ &= \frac{1}{\Delta t} \rho(x) \sum_{P'} p(x_1 - x'_{P'}), \end{aligned} \tag{11}$$

where we have used Eq. (8) in the second step. The sum in this equation accounts for the fact that the number of permutations P' accessible from any one permutation P may be

different than in the reverse direction. Let us define this number as

$$\mathcal{N}(x-x') \equiv \sum_{P'} H(x_P, x'_{P'}), \tag{12}$$

where

$$H(x_P, x'_{P'}) \equiv \begin{cases} 1 & \text{if } x'_{P'} \text{ is accessible from } x_P \\ 0 & \text{otherwise.} \end{cases} \tag{13}$$

Since $H(x_P, x'_{P'})$ need not be a symmetric function, $\mathcal{N}(x-x')$ may differ from $\mathcal{N}(x'-x)$. We then have

$$W(x-x') = \frac{1}{\Delta t}\mathcal{N}(x-x')\rho(x)p(x_1-x'_1), \tag{14}$$

if permutations are assigned such that x'_1 is accessible from x_1 in a single step. Here we have assumed that $p(x_1-x'_{P'})$ is the same for all accessible $x'_{P'}$, which is true for any algorithm that handles particle lists in a deterministic way.

To illustrate this point, consider a Monte Carlo move $x \to x'$ that attempts to insert a single particle, $N'=N+1$. If a particle is added to x_P, we need some convention for labeling the new particle position. For concreteness, we choose to place the new position at the end of the original list of positions, but all that is really required is that there is some deterministic scheme for introducing a new label. Thus there is a one-to-one relationship between P and P', and $\mathcal{N}(x-x')=1$. If, in the reverse move $x' \to x$, a particle is removed from $x'_{P'}$, and the remaining particles retain their original label ordering, then the label ordering in the resulting state x_P is again completely determined, and $\mathcal{N}(x'-x)=1$.

If two particles are added in a single Monte Carlo move, two different resulting computer states $x'_{P'}$, are possible, depending on the order in which the particles are added. Both states are reached with equal probability, and $\mathcal{N}(x-x')=2$. In the reverse move, however, with the deterministic removal scheme described above, the resulting state x_P is again completely determined, and $\mathcal{N}(x'-x)=1$.

In the ideal gas barostat, more than one particle may be inserted in a single step and particles may be added to the simulation in two distinct ways: They may be injected through the boundary of the atmosphere or they may appear in a lattice cell that has just been added to the simulation. Since multiple orderings of these particles are possible, one computer state x_P could generate many different permutations of the added particles in $x_{P'}$.

The number of distinct computer states $x_{P'}$ accessible from x_P is

$$\mathcal{N}(x-x') = N_{\text{in}}!N_{\text{app}}!. \tag{15}$$

Similarly,

$$\mathcal{N}(\bar{x}'-\bar{x}) = N_{\text{in}'}!N_{\text{app}'}!, \tag{16}$$

where "in′" and "app′" refer to particles added in the reverse step $\bar{x}' \to \bar{x}$. Particles that are removed from the simulation, either because they leave the atmosphere or because they are located in a cell that is no longer needed, need not be considered, as long as there is a deterministic removal scheme as discussed above.

Detailed balance requires that the net transition rates between two physical states are identical at equilibrium,

$$W(x-x') = W(\bar{x}'-\bar{x}). \tag{17}$$

Using Eq. (14), we can now write down the corresponding requirement for the permutation-specific transition probabilities as follows:

$$\frac{p(x_1-x'_1)}{p(\bar{x}'_1-\bar{x}_1)} = \frac{\rho(x')\mathcal{N}(\bar{x}'-\bar{x})}{\rho(x)\mathcal{N}(x-x')}. \tag{18}$$

Here we have used the fact that the stationary distribution of states is symmetric with respect to inversion of momenta, $\rho(\bar{x}')=\rho(x')$.

Inserting Eqs. (5), (15), and (16) into Eq. (18), we arrive at the final expression of the detailed balance condition as follows:

$$\frac{p(x_1-x'_1)}{p(\bar{x}'_1-\bar{x}_1)} = \frac{1}{h^{3\Delta N}}\frac{N_{\text{in}'}!N_{\text{app}'}!}{N_{\text{in}}!N_{\text{app}}!}e^{-\beta(\Delta U+P\Delta V-\mu\Delta N)}, \tag{19}$$

where $\Delta N=N'-N$, $\Delta U=U'-U$, and $\Delta V=V'-V$ are the differences in particle number, energy, and volume, respectively, between the states x and x'.

B. Transition probabilities

We proceed by explicitly calculating the transition probabilities for the ideal gas barostat. The transition probability from computer state x_1 to computer state x'_1 can be written as

$$p(x_1-x'_1) = \mathcal{P}_{\text{in}}(N_{\text{in}})\mathcal{P}_{\text{app}}(N_{\text{app}})\prod_{i\in\text{in}} f_{\text{in}}(\mathbf{q}'_i,\mathbf{p}'_i)\prod_{j\in\text{app}} f_{\text{app}}(\mathbf{q}'_j,\mathbf{p}'_j). \tag{20}$$

Here, $\mathcal{P}_{\text{in}}(N_{\text{in}})$ and $\mathcal{P}_{\text{app}}(N_{\text{app}})$ are Poisson distributions governing the number of added particles. The positions $\mathbf{q}'$ and momenta $\mathbf{p}'$ of added particles are distributed according to $f_{\text{in}}(\mathbf{q}',\mathbf{p}')$ for injected particles and $f_{\text{app}}(\mathbf{q}',\mathbf{p}')$ for appearing particles. Note that we omit delta-function singularities, associated with deterministic time evolution, that appear symmetrically in $p(x_1-x'_1)$ and $p(x'_1-x_1)$. In particular, this concerns the deterministic motion of nanocrystal atoms. A detailed sketch illustrating the algorithm's treatment of the ideal gas is shown in Fig. 2. The following discussion separately treats the cases of particle injection and particle appearance.

1. Particle injection

N_{in} denotes the number of particles that are added to the system through the injection algorithm, where n_{in} particles are put on the boundary of the ideal gas atmosphere and then propagated into the system. The average number of those particles $\bar{n}_{\text{in}}$ is given by Eq. (2). However, in general $N_{\text{in}} \neq n_{\text{in}}$ because there is chance that when propagated a particle will fly through a corner and leave the system (see Fig. 2), in which case it is no longer considered. We denote the probability for a successful injection, averaged over all possible injection points on the boundary R, by Π_R.

Dropping the subscript "in" for the moment, the probability to try an insertion for a number of n particles is given by the Poisson distribution

$$\hat{\mathcal{P}}_{\mathrm{in}}(n) = \frac{\bar{n}^n e^{-\bar{n}}}{n!}. \tag{21}$$

To obtain the probability that a total of N particles survive the insertion process, we must sum over all possible realizations,

$$\mathcal{P}_{\mathrm{in}}(N) = \sum_{n=N}^{\infty} \hat{\mathcal{P}}_{\mathrm{in}}(n) \binom{n}{N} (\Pi_R)^N (1-\Pi_R)^{n-N}. \tag{22}$$

Resumming,

$$\begin{aligned}
\mathcal{P}_{\mathrm{in}}(N) &= \frac{(\Pi_R)^N e^{-\bar{n}}}{N!} \sum_{n=N}^{\infty} \frac{\bar{n}^n}{(n-N)!} (1-\Pi_R)^{n-N} \\
&= \frac{(\Pi_R)^N e^{-\bar{n}}}{N!} \sum_{a=0}^{\infty} \frac{\bar{n}^{N+a}}{a!} (1-\Pi_R)^a \\
&= \frac{(\bar{n}\Pi_R)^N e^{-\bar{n}}}{N!} \sum_{a=0}^{\infty} \frac{\bar{n}^a}{a!} (1-\Pi_R)^a \\
&= \frac{(\bar{n}\Pi_R)^N e^{-\bar{n}}}{N!} e^{\bar{n}(1-\Pi_R)},
\end{aligned} \tag{23}$$

we end up with another Poisson distribution

$$\mathcal{P}_{\mathrm{in}}(N_{\mathrm{in}}) = \frac{\bar{N}_{\mathrm{in}}^{N_{\mathrm{in}}} e^{-\bar{N}_{\mathrm{in}}}}{N_{\mathrm{in}}!}, \tag{24}$$

with an average number of surviving particles

$$\bar{N}_{\mathrm{in}} = \bar{n}_{\mathrm{in}} \Pi_R. \tag{25}$$

For the evaluation of $f_{\mathrm{in}}(\mathbf{q},\mathbf{p})$ we adopt a coordinate system with respect to the local boundary of the ideal gas system, with $\mathbf{n}_x$ denoting the local unit normal to the boundary, pointing into the system. In our injection algorithm, a particle's position $\hat{\mathbf{q}}$ with components $(\hat{x},\hat{y},\hat{z})$ is assigned randomly, with $\hat{y}$ and $\hat{z}$ equidistributed on an area A with fixed coordinate $\hat{x}=x_0$. A momentum $\hat{\mathbf{p}}$ is drawn from a distribution $\varphi(\hat{\mathbf{p}})$, along with a time step τ, equidistributed within $(0,\Delta t)$. Then the particle is propagated to a new position $\mathbf{q}=\hat{\mathbf{q}}+\tau\hat{\mathbf{p}}/m$. The distribution of the set of random variates $(\tau,\hat{y},\hat{z},\hat{\mathbf{p}})$ is given by

$$\hat{f}_{\mathrm{in}}(\tau,\hat{y},\hat{z},\hat{\mathbf{p}}) = \frac{\Theta(\tau)\Theta(\Delta t-\tau)}{\Delta t} \times \frac{h_R(\hat{y},\hat{z})}{A} \times \varphi(\hat{\mathbf{p}}), \tag{26}$$

where $\Theta(\tau)$ is the step function,

$$\Theta(\tau) = \begin{cases} 1 & \text{if } \tau \geqslant 0 \\ 0 & \text{if } \tau < 0, \end{cases} \tag{27}$$

$h_R(\hat{y},\hat{z})$ is the characteristic function of the boundary R,

$$h_R(\hat{y},\hat{z}) = \begin{cases} 1 & \text{if } (\hat{y},\hat{z}) \text{ lies on } R \\ 0 & \text{else}, \end{cases} \tag{28}$$

and $\varphi(\hat{\mathbf{p}})$ is the momentum distribution

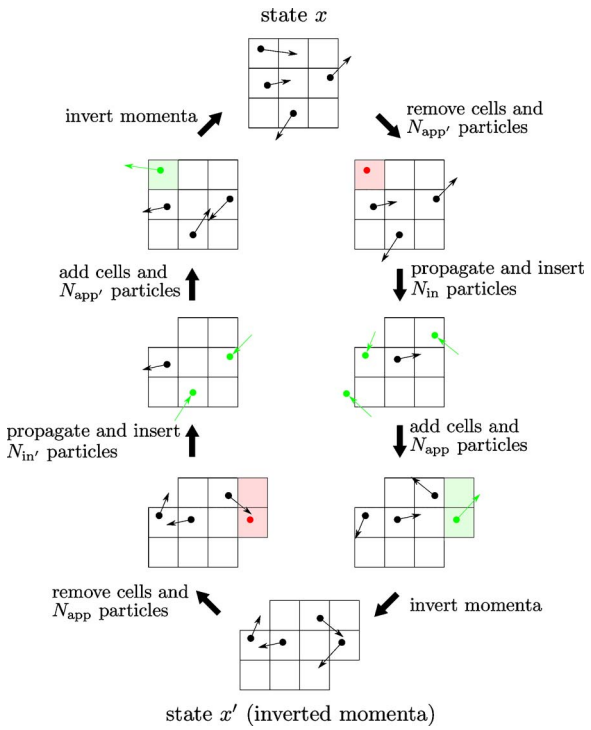

FIG. 2. Illustration of a transition between two states x and x' of the ideal gas system, nanocrystal not shown. The system starts in state x, with thin arrows indicating particle velocities. In the first step, unnecessary cells and particles therein (red) are removed. In the next step, particles are propagated according to their velocities; if they leave the atmosphere, they are no longer shown. New particles (green) are injected through the surface, with trailing velocity arrows indicating their imaginary positions one time step in the past. In the final step, new cells and particles (green) are added to the atmosphere. In the reverse move the same sequence of steps is passed. Note that in both directions particles are injected through the same boundary, and not all injected particles remain inside.

$$\varphi(\hat{\mathbf{p}}) = \frac{\beta^2}{2\pi m^2} \Theta(\hat{p}_x) \hat{p}_x e^{-\beta\hat{\mathbf{p}}^2/2m}. \tag{29}$$

We want to calculate the distribution of the position $\mathbf{q}=(x,y,z)$ and momentum $\mathbf{p}=(p_x,p_y,p_z)$ of an inserted particle. Thus we have to transform variables according to

$$\begin{aligned}
\tau &= (x-x_0)m/p_x, \\
\hat{y} &= y - p_y\tau/m = y - (x-x_0)p_y/p_x, \\
\hat{z} &= z - (x-x_0)p_z/p_x, \\
\hat{p}_x &= p_x, \\
\hat{p}_y &= p_y, \\
\hat{p}_z &= p_z.
\end{aligned} \tag{30}$$

An illustration of this transformation is shown in Fig. 3. With $\Delta x \equiv x - x_0$, the determinant of the Jacobian for this transformation reads

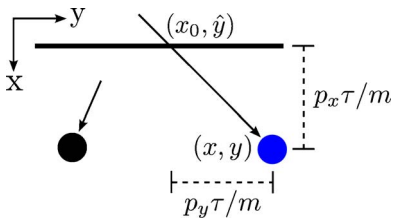

FIG. 3. Illustration of the variable transformation (30), z-direction not shown. The arrows indicate particle velocities, with arrows starting at particle positions one time step in the past. The blue gas atom was injected from the point $(x_0, \hat{y})$ on the surface, and propagated for a time τ to its final position (x, y). The other particle could not have reached its position through an injection event.

$$\begin{vmatrix} m/p_x & 0 & 0 & -\Delta x m/p_x^2 & 0 & 0 \\ -p_y/p_x & 1 & 0 & \Delta x p_y/p_x^2 & -\Delta x/p_x & 0 \\ -p_z/p_x & 0 & 1 & \Delta x p_y/p_x^2 & 0 & -\Delta x/p_x \\ 0 & 0 & 0 & 1 & 0 & 0 \\ 0 & 0 & 0 & 0 & 1 & 0 \\ 0 & 0 & 0 & 0 & 0 & 1 \end{vmatrix} = m/p_x. \tag{31}$$

Transforming the distribution $\hat{f}_{\text{in}}(\tau, \hat{y}, \hat{z}, \hat{\mathbf{p}})$ we arrive at

$$\tilde{f}_{\text{in}}(\mathbf{q},\mathbf{p}) = \frac{\varphi(\mathbf{p})}{A\Delta t p_x/m}\psi_R(\mathbf{q},\mathbf{p}) = \frac{\beta^2}{2\pi m A \Delta t} e^{-\beta \mathbf{p}^2/2m}\psi_R(\mathbf{q},\mathbf{p}), \tag{32}$$

where

$$\psi_R(\mathbf{q},\mathbf{p}) = \Theta[\tau(\mathbf{q},\mathbf{p})]\Theta[\Delta t - \tau(\mathbf{q},\mathbf{p})]\Theta(p_x) \times h_R[\hat{y}(\mathbf{q},\mathbf{p}), \hat{z}(\mathbf{q},\mathbf{p})] \tag{33}$$

decides, whether the set $(\mathbf{q},\mathbf{p})$ could have been produced by the insertion algorithm.

We are interested in the distribution $f_{\text{in}}(\mathbf{q},\mathbf{p})$ of particles that survive the insertion process only, yet $\tilde{f}_{\text{in}}(\mathbf{q},\mathbf{p})$ is nonzero for particles that end up out of bounds after the insertion process. To correct for these particles, we write

$$f_{\text{in}}(\mathbf{q},\mathbf{p}) = \frac{1}{\Pi_R}\tilde{f}_{\text{in}}(\mathbf{q},\mathbf{p})H_R(\mathbf{q}), \tag{34}$$

where

$$H_R(\mathbf{q}) = \begin{cases} 1 & \text{if } \mathbf{q} \text{ lies inside the boundary } R \\ 0 & \text{else} \end{cases} \tag{35}$$

is the characteristic function of the considered ideal gas volume. The normalizing constant Π_R, giving the probability that an insertion process will be successful, is obtained by integrating over phase space,

$$\Pi_R = \int \mathrm{d}\mathbf{q}\mathrm{d}\mathbf{p}\tilde{f}_{\text{in}}(\mathbf{q},\mathbf{p})H_R(\mathbf{q}). \tag{36}$$

The final expression for the probability distribution of positions and momenta of inserted particles then reads

$$f_{\text{in}}(\mathbf{q},\mathbf{p}) = \frac{\beta^2}{2\pi m A \Delta t \Pi_R} e^{-\beta \mathbf{p}^2/2m}\phi_R(\mathbf{q},\mathbf{p}), \tag{37}$$

where

$$\phi_R(\mathbf{q},\mathbf{p}) = \psi_R(\mathbf{q},\mathbf{p})H_R(\mathbf{q}) \tag{38}$$

decides, whether the set $(\mathbf{q},\mathbf{p})$ could have been produced by a *successful* insertion move.

2. Volume change

The average number of particles $\bar{N}_{\text{app}}$ added to newly considered ideal gas regions is given by Eq. (4). This average fully specifies the Poisson distribution

$$\mathcal{P}_{\text{app}}(N_{\text{app}}) = \frac{\bar{N}_{\text{app}}^{N_{\text{app}}} e^{-\bar{N}_{\text{app}}}}{N_{\text{app}}!}. \tag{39}$$

The appearing particles are distributed uniformly throughout the added volume, and their momenta are Maxwell-Boltzmann distributed,

$$f_{\text{app}}(\mathbf{q},\mathbf{p}) = \frac{1}{V_{\text{app}}}\left(\frac{2\pi m}{\beta}\right)^{-3/2} e^{-\beta \mathbf{p}^2/2m}. \tag{40}$$

C. Detailed balance

Assembling Eqs. (24), (37), (39), and (40), we can now write the transition probability (20) in detail,

$$\begin{aligned} p(x_1 - x_1') = {} & \left(\frac{\beta^2}{2\pi m A \Delta t \Pi_R}\right)^{N_{\text{in}}}\left[\frac{1}{V_{\text{app}}}\left(\frac{2\pi m}{\beta}\right)^{-3/2}\right]^{N_{\text{app}}} e^{-\beta K_{\text{add}}} \\ & \times \frac{(PA\Delta t \Pi_R \sqrt{\beta/2\pi m})^{N_{\text{in}}} e^{-PA\Delta t \Pi_R \sqrt{\beta/2\pi m}}}{N_{\text{in}}!} \\ & \times \frac{(\beta P V_{\text{app}})^{N_{\text{app}}} e^{-\beta P V_{\text{app}}}}{N_{\text{app}}!} \prod_{j \in \text{in}} \phi_R(\mathbf{q}_j', \mathbf{p}_j'), \end{aligned} \tag{41}$$

where K_{add} is the total kinetic energy of incoming particles. The last term simply decides, whether a transition between states x and x' is possible within our injection algorithm. Note that we can omit this factor in comparing transition probabilities because it is symmetric with respect to x and x' in the sense that only particles for which an injection is possible are carried back through the boundary in one time step, if their momenta are inverted. Simplifying,

$$\begin{aligned} p(x_1 - x_1') = {} & e^{-\beta K_{\text{add}}} \\ & \times \left[\beta P\left(\frac{\beta}{2\pi m}\right)^{3/2}\right]^{N_{\text{app}}+N_{\text{in}}} \frac{e^{-\beta P V_{\text{app}} - PA\Delta t \Pi_R \sqrt{\beta/2\pi m}}}{N_{\text{in}}! N_{\text{app}}!}. \end{aligned} \tag{42}$$

Considering the fact that in the reverse move particles are injected through the same boundary R (see Fig. 2), the ratio of forward and backward rates then takes the form

$$\frac{p(x_1 - x_1')}{p(\bar{x}_1' - \bar{x}_1)} = e^{-\beta \Delta U}\left[\beta P\left(\frac{\beta}{2\pi m}\right)^{3/2}\right]^{\Delta N} e^{-\beta P \Delta V}\frac{N_{\text{in}}'! N_{\text{app}}'!}{N_{\text{in}}! N_{\text{app}}!}. \tag{43}$$

With the fugacity of the ideal gas,

$$e^{\beta\mu} = h^3 \beta P \left(\frac{\beta}{2\pi m} \right)^{3/2}, \tag{44}$$

we arrive at

$$\frac{p(x_1 - x_1')}{p(\bar{x}_1' - \bar{x}_1)} = \frac{e^{-\beta(\Delta U + P\Delta V - \mu \Delta N)}}{h^{3\Delta N}} \frac{N_{\text{in}'}! N_{\text{app}'}!}{N_{\text{in}}! N_{\text{app}}!}. \tag{45}$$

A comparison with Eq. (19) shows that our algorithm indeed satisfies detailed balance.

D. Other implementations of the barostat

We briefly discuss possible pitfalls that have to be avoided in the implementation of the ideal gas barostat.

As an essential and seemingly complicated feature of the algorithm presented in Sec. II, the boundary of the ideal gas atmosphere is updated in two different steps. Consequently, particles leave the atmosphere and are injected through the same boundary in forward and backward moves. To illustrate how detailed balance can be violated if this is not the case, consider the following simple algorithm, which is similar to the one used in an earlier paper.[19]

(1) Propagate all particles for one time step, remove particles that leave the atmosphere.
(2) Inject particles through the surface.
(3) Update the atmosphere: remove cells that are no longer needed and add new cells, filled with gas particles.

Clearly, in this algorithm particles are exchanged through a possibly different boundary in the backward move. Consider now a particle A that leaves the atmosphere and is removed from the simulation in step (1). If in step (3) a new cell is added adjacent to the place where A left in step (1), particle A must be restored in the new cell with its proper position and velocity, otherwise the reverse move is not possible and detailed balance is violated. For an illustration of this situation, see Fig. 4.

As a possible solution, gas atoms leaving the atmosphere into cells that will be added during the same time step should not be removed from the simulation. Furthermore, particle insertions in newly added cells should only be accepted if inversion of momentum will not carry the particle back into the original atmosphere in one time step. However, the algorithm presented in Sec. II can be implemented more efficiently than this alternative scheme.

IV. TRANSITION PATH SAMPLING

In this section we show how the ideal gas barostat can be used within the framework of transition path sampling to study rare events such as structural transformations in nanoparticles under pressure.

A. Transition path ensemble

Many interesting physical and chemical processes require the crossing of high free energy barriers. First order phase transitions near the thermodynamic transition point and chemical reactions are examples of such processes. In particular, structural transformations in nanocrystals display

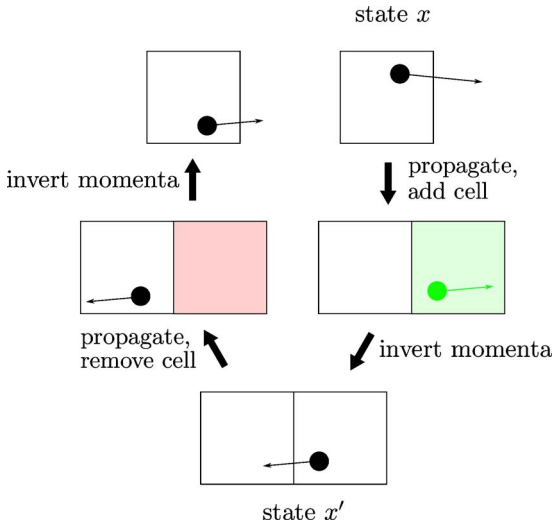

FIG. 4. Violation of detailed balance by a naive implementation of the ideal gas barostat, as described in the text. Starting in state x, the particle is propagated over the boundary and removed. A new cell is added and filled with a new gas particle (green) to form state x'. The reverse move, in which the added cell (red) is removed again, does not lead back to the original state x.

large hysteresis even on experimental time scales.[1,6] On time scales accessible in a straightforward molecular dynamics simulation, significantly higher pressures and pressurization rates must be applied to observe the transformation. At elevated pressures, however, the transformation mechanism can be different and the formation of grain boundaries is observed,[7,10] in contradiction with experiments.[1,6]

One generally applicable approach to spanning disparate time scales is transition path sampling.[20,21] Starting from an arbitrary trajectory displaying the transformation, a Monte Carlo procedure is used to generate an ensemble of reactive trajectories which can be analyzed to obtain the most probable transition path, the transition state, and even activation energies.[25] Because in a transition path simulation only reactive trajectories are considered, there is no need to artificially drive the system over the barrier and external parameters such as temperature and pressure need not be adjusted from experimental values.

The central object of transition path sampling is the ensemble of reactive trajectories that lead from region A to region B in phase space, perhaps crossing a large free energy barrier. We consider trajectories X of fixed length t, consisting of a sequence of L points in phase space separated by a time step Δt,

$$X = \{x_1, x_2, x_3, \ldots, x_L\}, \quad t = (L-1)\Delta t. \tag{46}$$

Note that x_i in this context denotes different physical states of the system along a trajectory, not different computer representations of a single physical state. The probability to observe a particular transition path is given by

$$\mathcal{P}(X) \propto h_A(x_1) h_B(x_L) \rho(x_1) \prod_{i=1}^{L-1} p(x_i - x_{i+1}). \tag{47}$$

Here, the characteristic functions $h_A(x_1)$ and $h_B(x_L)$ return unity only if the start and end points x_1 and x_L of the trajec-

tory lie in regions A and B, respectively, and zero otherwise; $\rho(x_1)$ is the probability density to observe the starting point, and the product gives the probability to move from one point along the trajectory to the next according to the dynamics of the system. In the case of the ideal gas barostat, the functions ρ and p correspond to Eqs. (5) and (42), respectively.

To sample the ensemble of trajectories defined by Eq. (47), a Monte Carlo procedure is used in close analogy to conventional Monte Carlo sampling in configuration space. Starting from an existing reactive trajectory a new trajectory is created, which is then accepted or rejected according to its probability relative to the old path. However, while trajectory space is sampled with a strong bias, the underlying dynamics of the system remain unaltered. As a result, trajectories obtained from a transition path sampling simulation are true dynamical trajectories, each evolving in time free of any bias.

B. Shooting and shifting

Two kinds of Monte Carlo moves are typically used to create new dynamical trajectories from old ones.[20] For a nanoparticle in the ideal gas pressure bath they take the following form.

In the first move, called *shooting*, a random point along a given trajectory is selected, dividing the trajectory in to two parts. Then, applying the algorithm described in Sec. II, a new trajectory is obtained by propagating the shooting point forward and backward in time. Because of the stochastic nature of the pressure bath, new gas particles are introduced on the surface of the atmosphere every time step and the new trajectory will eventually diverge from the old one. To increase the probability of generating a new trajectory that still leads from A to B, it is advisable to regrow only one part of the old trajectory, either forward or backward in time.

In the second move, the *shifting move*, the trajectory is extended forward or backward for a random period of time, and a segment of equal length is removed from the other end of the trajectory.

In one of the review papers on transition path sampling[20] it has been shown that for stochastic dynamics, under fairly general conditions, the above procedures result in correct sampling of Eq. (47) with a very simple acceptance rule: new trajectories are accepted if they still connect regions A and B, and rejected otherwise. The corresponding acceptance probability takes the form

$$\mathrm{acc}(X - X') = h_A(x_1')h_B(x_L'). \tag{48}$$

While systems such as the ideal gas barostat, where the total number of particles is not constant, were not explicitly considered in Ref. 20, the above acceptance probability is correct provided the underlying dynamics of the system satisfy the condition of microscopic reversibility,

$$\frac{p(x - x')}{p(\bar{x}' - \bar{x})} = \frac{\rho(x')}{\rho(x)}. \tag{49}$$

Again, the state $\bar{x}$ is obtained by inverting the momenta of all particles in state x. As we have shown in Sec. III, the ideal gas barostat fullfills this condition. Therefore the described shooting and shifting moves together with the simple acceptance criterion (48) result in correct sampling of trajectories.

V. SIMULATION RESULTS

In this section we apply the transition path sampling algorithm presented above to identify the primary mechanism of the h-MgO to rocksalt transformation in faceted CdSe nanocrystals.

Bulk CdSe transforms from the four-coordinate wurtzite to the six-coordinate rocksalt structure at a pressure of about 2.5 GPa.[26] In a recent paper, Shimojo *et al.*[16] studied this transformation in molecular dynamics computer simulation of a bulk crystal and identified two main mechanisms. In the first one the crystal is compressed in one of the equivalent [100] directions: the corresponding parallel (100) planes are flattened out and additional bonds are formed between atoms across six-membered hexagonal rings. This particular transformation route was first proposed by Tolbert and Alivisatos[1] for CdSe nanocrystals and will be called compression mechanism in the following. The second mechanism involves the sequential sliding of parallel (100) planes, where the 120° hexagonal bond angle along the planes is transformed into the 90° cubic angle. As a precursor to both mechanisms, the puckered (001) wurtzite layers are flattened out and the hexagonal five-coordinated h-MgO structure is formed as a metastable intermediate. Using transition path sampling, Zahn *et al.*[17] recently showed that in the bulk crystal near the thermodynamic transition pressure of 2.5 GPa the sliding plane mechanism is highly favored over the compression mechanism and the transition occurs via nucleation and growth.

In CdSe nanocrystals, the analogous transformation is strongly influenced by surface structure and size of the crystals.[7,12,14,27] Recent molecular dynamics simulations revealed that while spherical crystals transform much as observed in the bulk, the five-coordinated h-MgO structure can be stabilized in faceted crystals due to favorable surface energetics.[7,19] However, in both faceted and spherical crystals the transformation from the hexagonal to the cubic structure can proceed through either the compression or the sliding plane mechanism, or a mixture of both.[7,12,14]

To clarify the role of the two different mechanisms near the thermodynamic transition pressure, we apply the transition path sampling algorithm presented in the preceding section to the h-MgO to rocksalt transformation in faceted CdSe nanocrystals. While this transformation is observed at pressures of about 5.5 GPa in conventional molecular dynamics simulations, we here set the pressure to the bulk value of 2.5 GPa. We use the empirical pair potential for CdSe developed by Rabani.[28] Faceted $Cd_{216}Se_{216}$, $Cd_{528}Se_{528}$, and $Cd_{1050}Se_{1050}$ crystals with aspect ratios of about 1.0 are prepared by cleaving a bulk h-MgO lattice along equivalent (100) planes, with (001) and $(00\bar{1})$ planes terminating the crystals along the hexagonal [001] c-axis. We use trajectories of 20 ps length and a time step of 2 fs. At a temperature of 300 K, 44 000 gas particles are needed on average to apply a pressure of 2.5 GPa on a $Cd_{528}Se_{528}$ crystal.

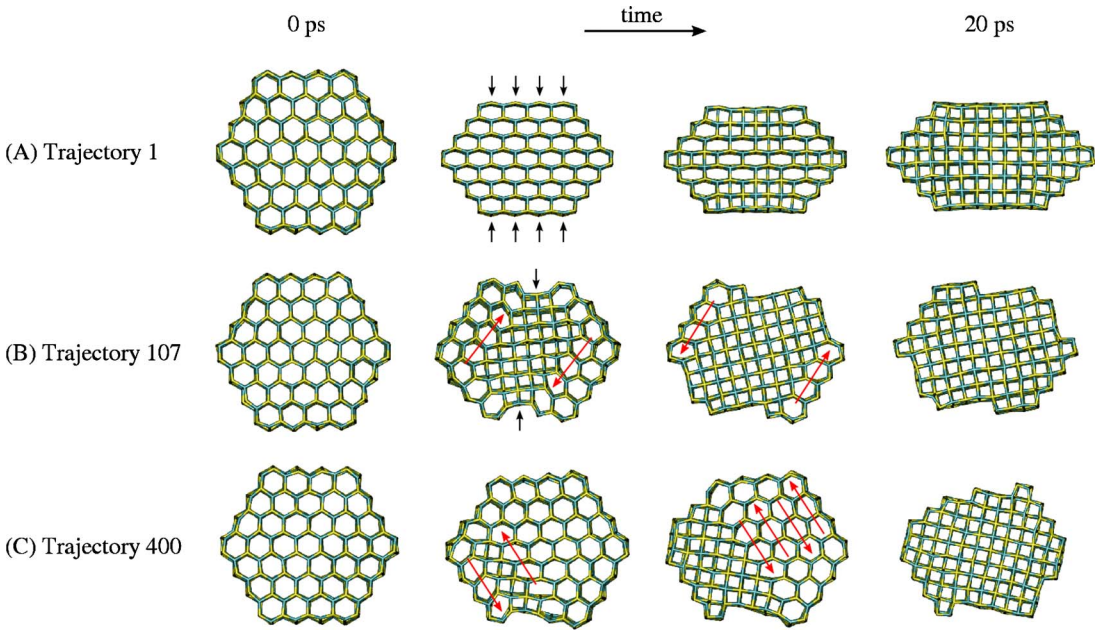

FIG. 5. Evolution of the transformation mechanism during a transition path sampling simulation of a $Cd_{528}Se_{528}$ crystal. Rows (A), (B), and (C) show three selected trajectories, each evolving in time from left to right, showing the crystal along the hexagonal *c*-axis. In all three trajectories the crystal has the *h*-MgO structure at 0 ps; 20 ps later it is found in the rocksalt structure. (A) The simulation starts from an artificial trajectory, where the crystal is transformed through a uniform compression in the direction orthogonal to one set of parallel (100) surfaces, as indicated by the black arrows. Atoms at opposite vertices of hexagonal six-membered rings come together to form an additional bond. (B) After approximately 100 shooting moves, the mechanism changes: The first part of the transformation still follows a similar route, rearranging the midsection of the crystal through the compression mechanism (black arrows). But then a different process begins, indicated by red arrows, which involves the sliding of parallel (100) planes. Note the different orientations of the final rocksalt lattice relative to the initial hexagonal lattice. (C) Yet a few hundred shooting moves later, the first mechanism has completely vanished and the crystal is transformed via the pure sliding plane mechanism. Starting on the surface, parallel (100) planes sequentially slide to transform the crystal, with adjacent planes preferably sliding in alternate directions.

The transformation is monitored by calculating the percentage of crystal atoms with six nearest neighbors. Atoms are defined to be nearest neighbors if they are closer than 3.3 Å, the location of the first minimum of the radial distribution function. We accept trajectories if the crystal has no six-coordinated atoms initially and 20 ps later has more than 28%, 45%, and 54% six-coordinated atoms for $Cd_{216}Se_{216}$, $Cd_{528}Se_{528}$, and $Cd_{1050}Se_{1050}$ crystals, respectively. These values were determined from straightforward simulations in the rocksalt structure.

A first trajectory, necessary for starting a transition path sampling simulation, is obtained in the following way: Positions $\mathbf{q}_0$ of crystal atoms are initialized according to $\mathbf{q}_0=(\mathbf{q}_{\mathrm{MgO}}+\mathbf{q}_{\mathrm{rs}})/2$, where $\mathbf{q}_{\mathrm{MgO}}$ represents the perfect *h*-MgO crystal and $\mathbf{q}_{\mathrm{rs}}$ are the positions of atoms in a rocksalt crystal obtained from a transformation via the compression mechanism. Particle velocities $\mathbf{p}_0$ are set to $\mathbf{p}_0=(\mathbf{q}_{\mathrm{rs}}-\mathbf{q}_{\mathrm{MgO}})/\Delta t$ and then scaled to a temperature of 300 K. Keeping crystal atoms fixed, the atmosphere of ideal gas particles around the crystal is allowed to equilibrate for 10 ps. Starting from this point, a first trajectory is obtained by propagating the system forward and backward in time, resulting in a transformation of the crystal via the compression mechanism.

Crystals of all three sizes qualitatively show the same behavior. A typical transition path sampling run for a $Cd_{528}Se_{528}$ is illustrated in Fig. 5. Starting with the pure compression mechanism involving a uniform motion of all crystal atoms, within a few hundred trajectories the transformation evolves towards the sliding plane mechanism, nucleating on the surface of the crystal and growing along parallel (100) planes. In the thousands of subsequent trajectories we harvested this mechanism persists: While the relative directions of sliding planes can vary, resulting in different shapes of the final rocksalt crystal, the mechanism does not change qualitatively. This result strongly suggests that near the thermodynamic transition pressure the sliding plane mechanism is the most favorable transition route.

ACKNOWLEDGMENTS

We thank Paul Alivisatos, Maxwell Merkle, Eran Rabani, and Josh Wittenberg for useful discussions. This work was supported by the Austrian Science Fund (FWF) within the Science College "Computational Materials Science" under Grant No. W004.

[1] S. H. Tolbert and A. P. Alivisatos, J. Chem. Phys. **102**, 4642 (1995).
[2] S. H. Tolbert, A. B. Herhold, L. E. Brus, and A. P. Alivisatos, Phys. Rev. Lett. **76**, 4384 (1996).
[3] J. Z. Jiang, J. S. Olsen, L. Gerward, D. Frost, D. Rubie, and J. Peyronneau, Europhys. Lett. **50**, 48 (2000).
[4] J.-E. Jørgensen, J. M. Jakobsen, J. Z. Jiang, L. Gerward, and J. S. Olsen, J. Appl. Crystallogr. **36**, 920 (2003).
[5] S. M. Clark, S. G. Prilliman, C. K. Erdonmez, and A. P. Alivisatos, Nanotechnology **16**, 2813 (2005).
[6] K. Jacobs, D. Zaziski, E. C. Scher, A. B. Herhold, and A. P. Alivisatos, Science **293**, 1803 (2001).
[7] M. Grünwald, E. Rabani, and C. Dellago, Phys. Rev. Lett. **96**, 255701 (2006).

[8] R. Martoňák, L. Colombo, C. Molteni, and M. Parrinello, J. Chem. Phys. **117**, 11329 (2002).
[9] S. Kodiyalam, R. K. Kalia, H. Kikuchi, A. Nakano, F. Shimojo, and P. Vashishta, Phys. Rev. Lett. **86**, 55 (2001).
[10] S. Kodiyalam, R. K. Kalia, A. Nakano, and P. Vashishta, Phys. Rev. Lett. **93**, 203401 (2004).
[11] B. J. Morgan and P. A. Madden, Nano Lett. **4**, 1581 (2004).
[12] B. J. Morgan and P. A. Madden, Phys. Chem. Chem. Phys. **8**, 3304 (2006).
[13] A. J. Kulkarni, M. Zhou, K. Sarasamak, and S. Limpijumnong, Phys. Rev. Lett. **97**, 105502 (2006).
[14] N. J. Lee, R. K. Kalia, A. Nakano, and P. Vashishta, Appl. Phys. Lett. **89**, 093101 (2006).
[15] M. Wilson and P. A. Madden, J. Phys.: Condens. Matter **14**, 4629 (2002).
[16] F. Shimojo, S. Kodiyalam, I. Ebbsjö, R. K. Kalia, A. Nakano, and P. Vashishta, Phys. Rev. B **70**, 184111 (2004).
[17] D. Zahn, Y. Grin, and S. Leoni, Phys. Rev. B **72**, 064110 (2005).
[18] S. E. Baltazar, A. H. Romero, J. K. Rodríguez-López, H. Terrones, and R. Martoňák, Comput. Mater. Sci. **37**, 526 (2006).
[19] M. Grünwald and C. Dellago, Mol. Phys. **104**, 3709 (2006).
[20] C. Dellago, P. G. Bolhuis, and P. L. Geissler, Adv. Chem. Phys. **123**, 1 (2002).
[21] C. Dellago, P. G. Bolhuis, F. S. Csajka, and D. Chandler, J. Chem. Phys. **108**, 1964 (1998).
[22] D. Frenkel and B. Smit, *Understanding Molecular Simulation* (Academic, New York, 2002).
[23] A. Malevanets and R. Kapral, J. Chem. Phys. **112**, 7260 (2000).
[24] C. W. Gardiner, *Handbook of Stochastic Methods: For Physics, Chemistry and the Natural Sciences* (Springer, Berlin, 2004).
[25] C. Dellago and P. G. Bolhuis, Mol. Simul. **30**, 795 (2004).
[26] H. Sowa, Solid State Sci. **7**, 1384 (2005).
[27] B. J. Morgan and P. A. Madden, J. Phys. Chem. C. **111**, 6724 (2007).
[28] E. Rabani, J. Chem. Phys. **116**, 258 (2002).